



In-situ extended X-ray absorption fine structure study of electrostriction in Gd doped ceria

Roman Korobko, Alyssa Lerner, Yuanyuan Li, Ellen Wachtel, Anatoly I. Frenkel, and Igor Lubomirsky

Citation: [Applied Physics Letters](#) **106**, 042904 (2015); doi: 10.1063/1.4906857

View online: <http://dx.doi.org/10.1063/1.4906857>

View Table of Contents: <http://scitation.aip.org/content/aip/journal/apl/106/4?ver=pdfcov>

Published by the [AIP Publishing](#)

Articles you may be interested in

[Local structure and polarization resistance of Ce doped SrMnO₃ using extended x-ray fine structure analysis](#)
Appl. Phys. Lett. **105**, 111903 (2014); 10.1063/1.4896107

[Extended X-ray absorption fine structure spectroscopy of selenium-hyperdoped silicon](#)
J. Appl. Phys. **114**, 133507 (2013); 10.1063/1.4824279

[Extended X-ray absorption fine structure study of Gd doped ZrO₂ systems](#)
J. Appl. Phys. **113**, 043508 (2013); 10.1063/1.4788823


[Phosphorus-doped silicon nanowires studied by near edge x-ray absorption fine structure spectroscopy](#)
Appl. Phys. Lett. **80**, 3709 (2002); 10.1063/1.1478796


[Fully relativistic theory for the magnetic extended x-ray absorption fine structure](#)
J. Appl. Phys. **83**, 7082 (1998); 10.1063/1.367853


A banner for Applied Physics Letters featuring the journal's logo and the text 'Meet The New Deputy Editors'. Below the text are three circular headshots of the new deputy editors: Alexander A. Balandin, Qing Hu, and David L. Price.

AIP | Applied Physics Letters

Meet The New Deputy Editors

 Alexander A. Balandin

 Qing Hu

 David L. Price

In-situ extended X-ray absorption fine structure study of electrostriction in Gd doped ceria

Roman Korobko,¹ Alyssa Lerner,² Yuanyuan Li,² Ellen Wachtel,¹ Anatoly I. Frenkel,^{2,a)} and Igor Lubomirsky^{1,b)}

¹Department of Materials and Interfaces, Weizmann Institute of Science, 234 Herzl Street, Rehovot 76100, Israel

²Physics Department, Yeshiva University, 245 Lexington Avenue, New York, New York 10016, USA

(Received 28 September 2014; accepted 15 January 2015; published online 29 January 2015)

Studying electric field-induced structural changes in ceramics is challenging due to the very small magnitude of the atomic displacements. We used differential X-ray absorption spectroscopy, an elementally specific and spatially sensitive method, to detect such changes in Gd-doped ceria, recently shown to exhibit giant electrostriction. We found that the large electrostrictive stress generation can be associated with a few percent of unusually short Ce-O chemical bonds that change their length and degree of order under an external electric field. The remainder of the lattice is reduced to the role of passive spectator. This mechanism is fundamentally different from that in electromechanically active materials currently in use. © 2015 AIP Publishing LLC.

[<http://dx.doi.org/10.1063/1.4906857>]

The electromechanical activity of the majority of piezoelectric and electrostrictive materials is due to cooperative ionic displacements throughout the crystal lattice.^{1–4} The magnitude of the electric field induced atomic displacements in these materials is related to their polarizability and, therefore, depends on the dielectric constant. Electrostrictors generally have large dielectric constants which, as in the case of lead magnesium niobates, can exceed 10 000.^{5,6} Recently, giant electrostriction, producing stress on the order of hundreds of MPa, was reported in thin films of 20 at. % Gd-doped ceria ($\text{Ce}_{0.8}\text{Gd}_{0.2}\text{O}_{1.9}$).⁷ a quadratic field dependence was observed over the complete range of electric field (0–100 kV/cm) and stress (0–500 MPa) investigated. Gd-doped ceria is one of the most extensively studied oxygen ion conductors.^{8–11} It has a dielectric constant < 30 ,¹² while the electrostriction polarization coefficient Q is (for $\text{Ce}_{0.8}\text{Gd}_{0.2}\text{O}_{1.9}$) $\approx 200 \text{ m}^4/\text{C}^2$ (Ref. 7) (Table I). This is orders of magnitude larger than any previously reported value.⁶ Such a combination of properties suggests that a distinctly different mechanism of electrostriction is at work, which—if identified—might refocus the search for electromechanically active materials. As we show below using *in situ* differential X-ray absorption spectroscopy (differential XAS), the structural changes associated with electric field-induced stress generation in ceria appear to be very different from those in other piezoelectric or electrostrictive materials.

For this study, 300–500 nm thick sputtered, strain-free films of $\text{Ce}_{1-x}\text{Gd}_x\text{O}_{2-x/2}$ ($x = 0.1, 0.2$ and 0.33) or $\text{CeO}_{2-\delta}$, sandwiched between 100 nm thick titanium electrodes, were prepared on (100) n-Si.¹³ Electrostriction coefficients of Gd-doped ceria films, measured using a cantilever deflection technique, show no dependence of electrostriction coefficient on field strength $\leq 60 \text{ kV/cm}$ (Ref. 7). Under field, all films exhibit in-plane expansion which, given the reported unrelaxed Poisson ratio,¹⁴ must be accompanied by reduction in

film thickness. Notably, this behavior is opposite to that of the most common electrostrictors.¹⁵ $\text{CeO}_{1.96\pm 0.1}$ films, in which 2% of the oxygen sites are vacant, also exhibit a relatively large electrostriction coefficient (Table I). However, when the concentration of vacant oxygen sites is reduced to 0.5%, as in $\text{CeO}_{1.99\pm 0.1}$, the electrostriction coefficient is reduced by a factor of three, indicating that in ceria, vacancies are an essential component of electrostriction. By contrast, in perovskite piezoelectrics, vacancies are known to have a deleterious effect on electromechanical properties.^{16,17} Since oxygen vacancies constitute only a few percent of the lattice anion sites in lightly doped or reduced ceria, and the calculated field induced strain is $< 6 \times 10^{-4}$ (Table I), an analysis technique is required that has both the elemental specificity and spatial sensitivity necessary to characterize structural aspects of the electromechanical response. In this letter, we describe the use of *in situ* X-ray absorption spectroscopy (XAS) measurements which are sensitive to changes in the local atomic and electronic structure of strained systems¹⁸ in the presence of a periodic electric field. Differential (“field on” minus “field off”) XAS detects only active species that respond to the electric field; passive (spectator) species do not contribute to the differential signal. This approach has been used previously in a number of studies, including those on magnetostriction,¹⁹ catalytic and electrocatalytic activity,^{20–23} and Ar-induced surface restructuring of Pd nanoclusters.²⁴

XAS measurements of the Ce and Gd L_{III} -edges were performed on the Gd-doped ceria electrostriction samples in fluorescence mode with a focused X-ray beam, spot size $\sim 1 \text{ mm}^2$.¹³ An electric field of $\sim 60 \text{ kV/cm}$ was periodically turned on for 45 s and off for an additional 45 s. These *on* and *off* cycles were repeated 10 times. During each half-cycle (*on* or *off*), 16–20 full XAS spectra were recorded. An eccentric-cam driven monochromator was used to continuously change the X-ray energy with a 1 scan/s data acquisition rate. This rate was necessary in order to minimize the possible influences of mechanical and/or dielectric

a) Anatoly.Frenkel@yu.edu

b) Igor.Lubomirsky@weizmann.ac.il

TABLE I. Electrostriction performance of 300–500 nm thick films of $\text{Ce}_{1-x}\text{Gd}_x\text{O}_{2-x/2}$ and $\text{CeO}_{2-\delta}$.^{7,13} $\%V_O$ is the oxygen vacancy concentration; σ is the measured electrostrictive stress with electric field $E \sim 60$ kV/cm. $\gamma = \sigma/E^2$ is the experimental electrostriction stress-field coefficient. Equivalent in-plane strain, $u_{xx} = \sigma \times (1 - \nu)/Y$. $M = u_{xx}/E^2$ and $Q = M/[\epsilon_0(\epsilon - 1)]^2$ electrostriction coefficients were calculated for the dielectric constant $\epsilon = 28$, unrelaxed elastic modulus $Y = 210 \pm 15$ GPa, and Poisson ratio $\nu = 0.28$.^{14,34,35}

	$\%V_O$	σ (MPa)	γ , (kPa/(kV/cm) ²)	u_{xx} , $\times 10^{-4}$	M , $m^2/V^2 \times 10^{-18}$	Q , m^4/C^2
$\text{CeO}_{1.99 \pm 1}$	0.5	25 ± 2	7 ± 1	0.8 ± 0.08	2.2 ± 0.21	39 ± 3.7
$\text{CeO}_{1.96 \pm 1}$	2	65 ± 3	18 ± 2	2 ± 0.1	5.8 ± 0.4	102 ± 7
$\text{Ce}_{0.9}\text{Gd}_{0.1}\text{O}_{1.95}$	2.5	180 ± 7	50 ± 4	5.8 ± 0.4	16 ± 1	282 ± 17
$\text{Ce}_{0.8}\text{Gd}_{0.2}\text{O}_{1.90}$	5	101 ± 4	28 ± 1	3.2 ± 0.2	9 ± 0.6	157 ± 10
$\text{Ce}_{0.67}\text{Gd}_{0.33}\text{O}_{1.835}$	8.25	173 ± 5	48 ± 1	5.6 ± 0.3	15.5 ± 0.9	271 ± 15

time-dependent relaxation. After removing 3–5 spectra at the beginning of each *on* or *off* half-cycle, to eliminate transient states, the remaining spectra were normalized and merged. The final data set for each sample contained 10 pairs of average spectra—*on* and *off*—for the Ce and Gd L_{III}-edges. Figures 1(a) and 1(b) show representative X-ray absorption near edge spectra (XANES) for one cycle for $\text{Ce}_{0.9}\text{Gd}_{0.1}\text{O}_{1.95}$. The Ce L_{III}-edge white line comprises two prominent Ce^{4+} peaks: A ($2p_- 4f^0 5d^1$ state) and B ($2p_- 4f^1 5d^1 L_-$ state), where $2p_-$ denotes the empty state in the 2p shell and L_- denotes an empty state in the neighboring oxygen orbital.²⁵ The intensity of both peaks is observed to increase under applied field, while the intensity of the Gd white line remains unchanged. To obtain the differential XANES (Δ XANES) signal, the merged spectra in the *off*-state half cycle were subtracted from the corresponding merged *on*-state spectra for each of the three Gd doping levels and for each element, i.e., Ce and Gd. Integration of the differential signals was performed within the 25 eV range for each edge data (5715–5740 eV for Ce and 7235–7260 eV for Gd) and the resulting areas plotted for each of the ten cycles (Figs. 1(c) and 1(d)). It is clear that only the environment of the Ce ion is affected by the electric field, with the largest signal coming from the 10 at. % Gd sample. We interpret the increase in integrated intensity of the white line in the *on*

half-cycle as being due to increase in the density of unoccupied states of Ce as a result of increased ionic character, stronger configurational order, and/or greater coordination number of neighbors.^{7,25} By normalizing both the Ce Δ XANES signal, averaged over 10 cycles, and the electrostriction stress coefficient of each sample (Table I) to the concentration of oxygen vacancies, a clear relationship is observed (Fig. 2) between the electromechanical performance of the material as a whole and local changes in those chemical species which respond to application of an electric field.

Extended X-ray absorption fine structure (EXAFS) measurements are complementary to XANES and provide additional structural details. The EXAFS spectra of the ceria films were analyzed as described in the supplementary material.¹³ Differential EXAFS spectra,

$$\Delta\chi = \chi(E_{on}) - \chi(E_{off}), \quad (1)$$

where $\chi(E_{on \text{ or } off}) = \chi_{\text{spectator}} + \chi_{\text{active}}(E_{on \text{ or } off})$ is the total EXAFS signal, contain information only about *active* bonds, i.e., those bonds that are modified during field *on* or *off* switching. The differential EXAFS signal, $\Delta\chi$, was obtained by subtracting the averaged spectra measured in the *off* half-cycle from the averaged spectra measured in the *on*

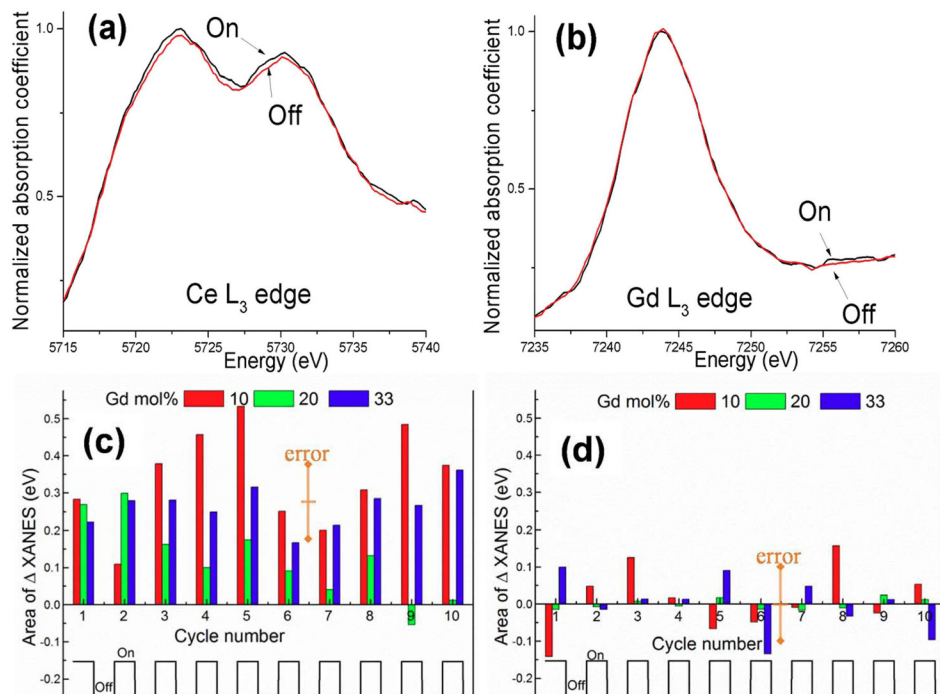


FIG. 1. Representative XANES L_{III}-edge data for a 10 at. % Gd doped ceria film in the white line region of Ce (a) and Gd (b) for a pair of successive field *on*-states (black curve) and *off*-states (red curve). Merged integrated areas of the differential Ce (c) and Gd (d) Δ XANES signals measured in each of the ten on-off cycles. The estimated standard error of the mean is ± 0.1 eV for each cycle.

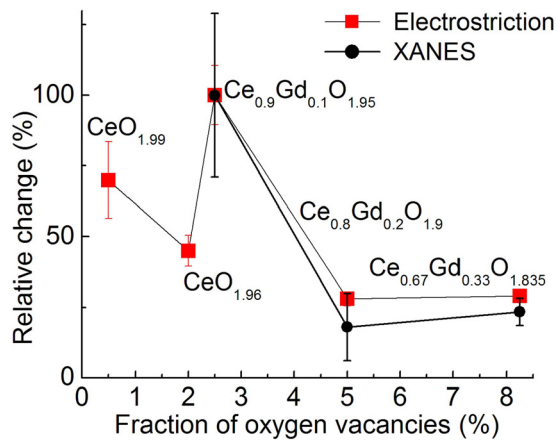


FIG. 2. The differential XANES signal for the Ce L_{III} edge averaged over 10 electric field *on-off* cycles (●) and the electrostriction stress coefficient (■), both normalized by the % oxygen vacancies. The respective values for 10 at. % Gd doped ceria are taken as 100%.

half-cycle and then averaging the difference over 10 cycles. Figure 3(a) presents the k -weighted spectrum $\Delta\chi$ as a function of k , the photoelectron wave number, for the $\text{Ce}_{0.9}\text{Gd}_{0.1}\text{O}_{1.95}$ film. As noted above, this sample has the largest electrostriction stress coefficient, as well as the largest ΔXANES signal. $\Delta\chi$ for the Ce L_{III} -edge could not be reliably measured for the other samples, perhaps because the structural change per oxygen vacancy was below the detection limit (Fig. 2), even though the overall electromechanical stress is significant (Table I). We note also that $\Delta\chi$ for the Gd L_{III} -edge was negligible. A model can be fit to the experimental spectrum $\Delta\chi(k)$ according to the standard EXAFS plane wave expansion

$$\chi_{\text{model}} = \frac{NS_0^2}{kR^2} e^{-2k^2\sigma^2} e^{-2R/\lambda} f(k) \sin\left(2kR - \frac{4}{3}C_3k^3 + \delta(k)\right), \quad (2)$$

where N and R are the coordination number and bond length for the nearest neighbors to Ce; S_0^2 is the amplitude factor for Ce;¹³ λ is the photoelectron mean free path; σ^2 is the mean squared disorder in Ce-O bond length; $f(k)$ is the backscattering amplitude; and $\delta(k)$ is a phase shift. C_3 is the anharmonic correction to the effective pair potential that characterizes the asymmetry of the pair distribution function.²⁶ Due to the

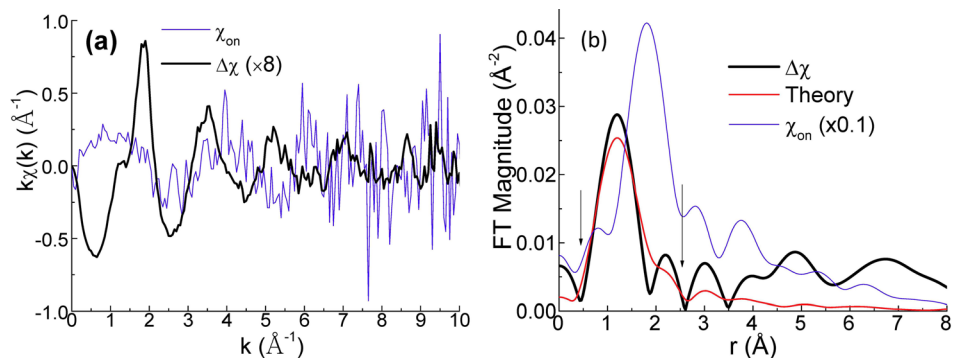


FIG. 3. (a) Differential EXAFS k -weighted signal ($k\Delta\chi$) for a 10 at. % Gd-doped ceria film, averaged over 10 *on-off* cycles and the corresponding EXAFS signal averaged over 1 half-cycle ($k\chi_{\text{on}}$); (b) Magnitude of the Fourier transform of $\Delta\chi$; the best-fit model for $\Delta\chi$; and magnitude (scaled down by a factor of 0.1) of the Fourier transform of χ_{on} . The imaginary parts of the Fourier transforms of the data and theory are shown in the supplementary material Fig. S1.¹³ Arrows denote the fitting range in r -space.

difficulty introduced by the presence of multi-electron excitations and multiple scattering in Ce L_{III} -edge EXAFS, only the first coordination shell around Ce (nearest neighbor oxygen atoms) was fitted here.²⁷ Adjustable parameters were N , R , σ^2 , and C_3 . This form of the model spectrum may also be used to describe the appearance or disappearance of a minority population in the environment of Ce upon application of the electric field. The fitting of the theoretical model (Eq. (2)) to the measured $\Delta\chi$ was performed for k within the range $1.5\text{--}5.7 \text{ \AA}^{-1}$. The best-fit values for $\Delta\chi$ and χ_{on} (or χ_{off}) are shown in Table II. Fit values for a $\text{Ce}_{0.9}\text{Gd}_{0.1}\text{O}_{1.95}$ ceramic in the absence of an electric field are shown for comparison.²⁸ The magnitudes of the Fourier transform of experimental data and theoretical fits for both $\Delta\chi$ and $\Delta\chi_{\text{on}}$ are shown in Fig. 3(b). The best-fit result for the Ce-O bond length in the differential EXAFS signal was $2.22 \pm 0.09 \text{ \AA}$, and the effective Ce-O coordination number was found to be -0.26 ± 0.07 . Given that the differential signal is the difference between the *on* and the *off* states, the minus sign indicates that the short Ce-O bonds are not present in the *on* state. The average length of all Ce-O bonds was found to be $2.33 \pm 0.02 \text{ \AA}$ by EXAFS analysis of a typical χ_{on} (or χ_{off}) spectrum. In the field-*on* (or -*off*) state, the small population of electroactive bonds must be included in the average first coordination shell of Ce, but the limited sensitivity of the standard EXAFS analysis does not allow us to detect their contribution. The active Ce-O bonds were found to have anomalously high anharmonicity ($C_3 = 0.210 \pm 0.008 \text{ \AA}^3$), much larger than the value dominated by the spectator bonds ($C_3 = 0.000 \pm 0.002 \text{ \AA}^3$). These electro-active bonds are $\approx 4.6\%$ shorter than the average Ce-O bond in the lattice. When modified by the electric field, each creates local strain of up to 4.6%. Comparison of coordination numbers shows that the short bonds comprise $\approx 3.4\%$ of the total Ce-O bonds in the lattice. Therefore, they introduce a maximum overall strain into the lattice of $\approx 1.56 \times 10^{-3}$, which is more than sufficient to account for the experimental field-induced strain of $(5.8 \pm 0.4) \times 10^{-4}$ in $\text{Ce}_{0.9}\text{Gd}_{0.1}\text{O}_{1.95}$ (Table I).

Prior to this work, structural details of oxygen deficient ceria films were only reported in the absence of an electric field. Powder X-ray diffraction patterns from $\text{Ce}_{1-x}\text{Gd}_x\text{O}_{2-x/2}$ ($x \leq 0.2$) films can be indexed according to fluorite symmetry (Fm-3m). However, local deviations from the average

TABLE II. Fit parameters (Eq. (2)) for EXAFS spectra of $\text{Ce}_{0.9}\text{Gd}_{0.1}\text{O}_{1.95}$. N and R are the coordination number and bond length for the nearest neighbors (Ce-O bond); σ^2 is the mean squared disorder in the Ce-O bond length; C_3 is the anharmonic correction to the effective pair potential, and ΔE is the correction to the origin of the photoelectron energy.

	N	R (Å)	σ^2 (Å ²)	ΔE (eV)	C_3 (Å ³)
χ (on or off) film	7.6 ± 1.5	2.33 ± 0.02	0.014 ± 0.006	6.5	0.000 ± 0.002
χ (off) ceramic ²⁸	8 (fixed)	2.32	0.008 ± 0.001	7.6	0 ^a
$\Delta\chi$ (film)	-0.26 ± 0.07	2.22 ± 0.09	0.000 ± 0.008	7.6	0.210 ± 0.008

^aThis parameter was previously found not to affect the fit.

structure have been identified by EXAFS:²⁹ a decrease in the average Ce-near neighbor oxygen bond length, i.e., 2.341 Å (undoped) to 2.325 Å (20 at. % doped), and an enlarged Ce-oxygen vacancy (V_O) distance (2.62 ± 0.14 Å). Local symmetry reduction and shortening of Ce-O bonds^{28,30,31} in doped or reduced ceria have been attributed to the fact that electrostatic interactions promote relaxation of unscreened cations away from the vacant oxygen sites while remaining oxygen ions move towards them.³² Therefore, in the field-free case, although the eight oxygen atoms in the first coordination shell of Ce may display the cubic symmetry of the fluorite lattice, a $\text{Ce}_{\text{Ce}} - 7\text{O} - V_O$ complex may be distorted. In $\text{Ce}_{0.9}\text{Gd}_{0.1}\text{O}_{1.95}$, the probability that a Ce ion will have one near neighbor oxygen vacancy is 16.4%.¹³ Here, we find evidence from XAS that for a subset of Ce ions in Gd-doped ceria, this distortion of the near neighbor environment away from Fm-3m symmetry in the absence of an electric field is, in its presence, relieved.

We have previously considered a model of the $\text{Ce}_{\text{Ce}} - 7\text{O} - V_O$ complex:⁷ six oxygen atoms are shifted to positions closer to the Ce ion than in pure ceria, whereas the anion sites on the $\text{Ce}_{\text{Ce}} - V_O$ diagonal, i.e., the seventh oxygen atom and the oxygen vacancy, are more distant from the Ce ion (Fig. 4, *distorted* complex). This distortion from cubic symmetry produces an asymmetric charge distribution as well as a local dipolar elastic field³³ in the fluorite lattice: expansion along the $\text{Ce}_{\text{Ce}} - V_O$ direction and contraction in the planes nearly perpendicular to this direction. In the presence of an electric field, the model for $\Delta\chi$ that provided the best fit to experimental data shows that the length of the active, contracted Ce-O bonds (2.22 ± 0.09 Å) in a distorted complex increases towards the spectator-dominated average value (2.33 ± 0.02 Å) (Fig. 4, *cubic* complex). Removal of the field spontaneously restores the original distortion. Since the $\text{Ce}_{0.9}\text{Gd}_{0.1}\text{O}_{1.95}$ films display strong (111) texture,¹³ electromechanical coupling to the

elastic dipole would produce the strongest response for those complexes in which the highly polarizable $\text{Ce}_{\text{Ce}} - V_O$ direction is parallel (or antiparallel) to the [111] reciprocal lattice vector, i.e., perpendicular to the film plane. The result is in-plane expansion (as observed), and—assuming that the field-*on* $\text{Ce}_{\text{Ce}} - V_O$ distance is correspondingly reduced—out-of-plane contraction would also occur.

The electrostrictive behavior of Gd-doped or reduced ceria films provides a striking contrast to classical electrostrictors in which application of an electric field produces cooperative ionic displacements in the crystal lattice. Using EXAFS measurements and differential analysis, we have shown that the electric field generated stress in oxygen-deficient ceria can be associated with the response of a small population of strongly anharmonic chemical bonds. The differential XAS technique, performed under periodic perturbation with an electric field, improves sensitivity for real time detection to the extent that this minor population of electroactive bonds can be identified. Materials such as the fluorite oxides described here, which tolerate relatively large concentrations of oxygen vacancies interacting with host cations, may bring to the spotlight a previously unknown class of electromechanically active materials.

I.L. thanks the Minerva foundation and the US-Israel Binational Science Foundation for funding this research. I.L. specifically wishes to acknowledge the assistance of the Nancy and Stephen Grand Research Center for Sensors and Security. A.I.F. acknowledges support by the U.S. DOE (Grant No. DE-FG02-03ER15476). Beamline X18A at the NSLS is supported in part by the Synchrotron Catalysis Consortium (U.S. DOE Grant No. DE-FG02-05ER15688). In addition, A.L. acknowledges support by the Catalysis Center for Energy Innovation, an Energy Frontier Research Center funded by the U.S. Department of Energy, Office of Science, Office of Basic Energy Sciences under Award No. DE-SC0001004. The research is also made possible in part by the generosity of the Harold Perlman Family.

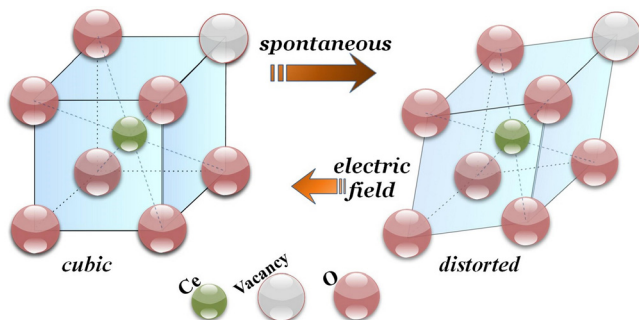


FIG. 4. Scheme of the electric field induced reorganization of a distorted Ce near neighbor coordination shell containing an oxygen vacancy.

¹D. Damjanovic, “Ferroelectric, dielectric and piezoelectric properties of ferroelectric thin films and ceramics,” *Rep. Prog. Phys.* **61**(9), 1267 (1998).

²P. Murali, R. G. Polcawich, and S. Trolier-McKinstry, “Piezoelectric thin films for sensors, actuators, and energy harvesting,” *Mrs Bull.* **34**(9), 658 (2009).

³M. T. Sebastian, H. Klapper, and R. J. Bolt, “X-ray-diffraction study of Ktp (Ktiop4) crystals under a static electric-field,” *J. Appl. Crystallogr.* **25**, 274 (1992).

⁴J. L. Jones, A. Pramanick, J. C. Nino, S. M. Motahari, E. Ustundag, M. R. Daymond, and E. C. Oliver, “Time-resolved and orientation-dependent electric-field-induced strains in lead zirconate titanate ceramics,” *Appl. Phys. Lett.* **90**(17), 172909 (2007).

- ⁵D. S. Fu, H. Taniguchi, M. Itoh, S. Koshihara, N. Yamamoto, and S. Mori, "Relaxor $\text{Pb}(\text{Mg}_{1/3}\text{Nb}_{2/3})\text{O}_3$: A ferroelectric with multiple inhomogeneities," *Phys. Rev. Lett.* **103**(20), 207601 (2009).
- ⁶R. E. Newnham, V. Sundar, R. Yimnirun, J. Su, and Q. M. Zhang, "Electrostriction: Nonlinear electromechanical coupling in solid dielectrics," *J. Phys. Chem. B* **101**(48), 10141 (1997).
- ⁷R. Korobko, A. Patlolla, A. Kossoy, E. Wachtel, H. L. Tuller, A. I. Frenkel, and I. Lubomirsky, "Giant electrostriction in Gd-doped ceria," *Adv. Mater.* **24**(43), 5857 (2012).
- ⁸J. L. Hertz, M. L. Di Vona, P. Knauth, and H. L. Tuller, "Advanced materials for fuel cells introduction," *J. Mater. Res.* **27**(15), 1905 (2012).
- ⁹J. L. M. Rupp, T. Drobek, A. Rossi, and L. J. Gauckler, "Chemical analysis of spray pyrolysis gadolinia-doped ceria electrolyte thin films for solid oxide fuel cells," *Chem. Mater.* **19**(5), 1134 (2007).
- ¹⁰M. Mogensen, N. M. Sammes, and G. A. Tompsett, "Physical, chemical and electrochemical properties of pure and doped ceria," *Solid State Ionics* **129**(1–4), 63 (2000).
- ¹¹H. Inaba and H. Tagawa, "Cerium-based solid electrolytes," *Solid State Ionics* **83**(1–2), 1 (1996).
- ¹²V. Shelukhin, I. Zon, E. Wachtel, Y. Feldman, and I. Lubomirsky, "Low temperature dielectric properties of $\text{Ce}_{0.8}\text{Gd}_{0.2}\text{O}_{1.9}$ films," *Solid State Ionics* **211**(0), 12 (2012).
- ¹³See supplementary material at <http://dx.doi.org/10.1063/1.4906857> for 1. Preparation of thin films; 2. XAS data collection and analysis; 3. Estimate of the number of Ce-O bonds modified by the electric field.
- ¹⁴A. Atkinson, "Chemically-induced stresses in gadolinium-doped ceria solid oxide fuel cell electrolytes," *Solid State Ionics* **95**(3–4), 249 (1997).
- ¹⁵R. A. Cowley, S. N. Gvasaliya, S. G. Lushnikov, B. Roessli, and G. M. Rotaru, "Relaxing with relaxors: a review of relaxor ferroelectrics," *Adv. Phys.* **60**(2), 229 (2011).
- ¹⁶P. Gao, C. T. Nelson, J. R. Jokisaari, S. H. Baek, C. W. Bark, Y. Zhang, E. G. Wang, D. G. Schlom, C. B. Eom, and X. Q. Pan, "Revealing the role of defects in ferroelectric switching with atomic resolution," *Nat. Commun.* **2**, 591 (2011).
- ¹⁷C. Verdier, F. D. Morrison, D. C. Lupascu, and J. F. Scott, "Fatigue studies in compensated bulk lead zirconate titanate," *J. Appl. Phys.* **97**(2), 024107 (2005).
- ¹⁸C. Lamberti, "The use of synchrotron radiation techniques in the characterization of strained semiconductor heterostructures and thin films," *Surf. Sci. Rep.* **53**(1–5), 1 (2004).
- ¹⁹R. F. Pettifer, O. Mathon, S. Pascarelli, M. D. Cooke, and M. R. J. Gibbs, "Measurement of femtometre-scale atomic displacements by X-ray absorption spectroscopy," *Nature* **435**(7038), 78 (2005).
- ²⁰C. F. J. Konig, J. A. van Bokhoven, T. J. Schildhauer, and M. Nachtgeaal, "Quantitative analysis of modulated excitation x-ray absorption spectra: Enhanced precision of EXAFS fitting," *J. Phys. Chem. C* **116**(37), 19857 (2012).
- ²¹C. Roth and D. E. Ramaker, *Fuel Cell Science* (John Wiley & Sons, Inc., 2010), p. 511.
- ²²D. E. Ramaker and D. C. Koningsberger, "The atomic AXAFS and $\Delta\mu$ XANES techniques as applied to heterogeneous catalysis and electrocatalysis," *Phys. Chem. Chem. Phys.* **12**(21), 5514 (2010).
- ²³D. E. Ramaker, D. Gatewood, A. Korovina, Y. Garsany, and K. E. Swider-Lyons, "Resolving sulfur oxidation and removal from Pt and Pt_3Co electrocatalysts using *in situ* x-ray absorption spectroscopy," *J. Phys. Chem. C* **114**(27), 11886 (2010).
- ²⁴C. S. Spanjers, T. P. Senftle, A. C. T. van Duin, M. J. Janik, A. I. Frenkel, and R. M. Rioux, "Illuminating surface atoms in nanoclusters by differential X-ray absorption spectroscopy," *Phys. Chem. Chem. Phys.* **16**, 26528 (2014).
- ²⁵F. Zhang, P. Wang, J. Koberstein, S. Khalid, and S. W. Chan, "Cerium oxidation state in ceria nanoparticles studied with X-ray photoelectron spectroscopy and absorption near edge spectroscopy," *Surf. Sci.* **563**(1–3), 74 (2004).
- ²⁶G. Dalba, P. Fornasini, M. Grazioli, R. Gotter, and F. Rocca, "EXAFS analysis for anharmonic systems," *Physica B* **208–209**(0), 135 (1995).
- ²⁷A. Kossoy, A. I. Frenkel, Y. Feldman, E. Wachtel, A. Milner, and I. Lubomirsky, "The origin of elastic anomalies in thin films of oxygen deficient ceria, CeO_{2-x} ," *Solid State Ionics* **181**(33–34), 1473 (2010).
- ²⁸A. Kossoy, Q. Wang, R. Korobko, V. Grover, Y. Feldman, E. Wachtel, A. K. Tyagi, A. I. Frenkel, and I. Lubomirsky, "Evolution of the local structure at the phase transition in $\text{CeO}_2\text{-Gd}_2\text{O}_3$ solid solutions," *Phys. Rev. B* **87**(5), 054101 (2013).
- ²⁹A. Kossoy, A. I. Frenkel, Q. Wang, E. Wachtel, and I. Lubomirsky, "Local structure and strain-induced distortion in $\text{Ce}_{0.8}\text{Gd}_{0.2}\text{O}_{1.9}$," *Adv. Mater.* **22**(14), 1659 (2010).
- ³⁰S. Yamazaki, T. Matsui, T. Sato, Y. Arita, and T. Nagasaki, "EXAFS study of reduced ceria doped with lanthanide oxides," *Solid State Ionics* **154**, 113 (2002).
- ³¹C. Artini, G. Costa, M. Pani, A. Lausi, and J. Plaisier, "Structural characterization of the $\text{CeO}_2/\text{Gd}_2\text{O}_3$ mixed system by synchrotron X-ray diffraction," *J. Solid State Chem.* **190**, 24 (2012).
- ³²D. Marrocchelli, S. R. Bishop, H. L. Tuller, and B. Yildiz, "Understanding chemical expansion in non-stoichiometric oxides: Ceria and zirconia case studies," *Adv. Funct. Mater.* **22**(9), 1958 (2012).
- ³³A. S. Nowick and B. S. Berry, *Anelastic Relaxation in Crystalline Solids* (Academic Press, 1972), p.704.
- ³⁴R. Korobko, S. K. Kim, S. Kim, S. R. Cohen, E. Wachtel, and I. Lubomirsky, "The role of point defects in the mechanical behavior of doped ceria probed by nanoindentation," *Adv. Funct. Mater.* **23**(48), 6076 (2013).
- ³⁵R. Korobko, C. T. Chen, S. Kim, S. R. Cohen, E. Wachtel, N. Yavo, and I. Lubomirsky, "Influence of Gd content on the room temperature mechanical properties of Gd-doped ceria," *Scr. Mater.* **66**(3–4), 155 (2012).